# Power Delay Profiles for a Wireless Endoscopy Link

W. Joseph*      E. Tanghe*      P. Van Torre†      G. Vermeeren*      S. Agneessens†

H. Rogier†        L. Martens*

*Abstract* — In this work, we investigate power delay profiles for a wireless in-to-out-body endoscopy link. A hospital scenario is considered where endoscopy images taken inside the body are wirelessly transmitted to a monitoring device outside the body. We distinguish between a direct in-to-out-body link and a dual-hop relay link where the image data is first sent to an on-body hub device. Path loss for the direct link is found to be fairly high to allow for reliable communication. It is argued that the dual-hop relay link is a better option because it offers options to alleviate the path loss issue, such as amplification or retransmission of data.

## 1 Introduction

In this paper, propagation aspects of a wireless endoscopy link in a hospital scenario are investigated. Practically, we think of a capsule camera that can be swallowed by the patient and is equipped to wirelessly transmit images to a receiving monitoring device in the vicinity of the patient. We distinguish between two possible ways of realizing the endoscopy link. We consider the direct link between the in-body capsule camera and the out-body monitoring device. Alternatively, we also consider a dual-hop relay link where the in-body images are first transmitted to an on-body hub device that in turn relays the data to the out-body terminal device. Propagation characteristics of the direct and relay links are investigated through measurements of the Averaged Power Delay Profile (APDP). The considered frequency band is the 2.4 GHz ISM band.

## 2 Measurements and data processing

A human body is simulated by means of a flat phantom that represents the average trunk of a human and is recommended by CENELEC standard EN50383 [1]. The phantom is filled with muscle tissue simulating fluid (relative permittivity = 50.8 and conductivity = 2.01 S/m at 2.45 GHz). A vector network analyzer is used to measure the $S_{21}$ parameter between transmitting antennas Tx

and receiving antennas Rx that represent the various communication links in the endoscopy scenario. The $S_{21}$ parameter is measured in a 280 MHz bandwidth from 2340 to 2620 MHz with a frequency step of 1 MHz.

Fig. 1 shows a top-down view of the measurement setup. The link between the in-body antenna $Tx_1$ and the on-body antenna $Rx_1$ is called 'hop 1'. In this setup, the orientation of the human trunk phantom is such that it simulates a person lying down horizontally in the XY-plane on e.g., a hospital bed. $Tx_1$ is moved along a 7 by 7 square grid in the liquid with 10 mm spacing between the grid points. This spacing is chosen as it is larger than half a wavelength inside the liquid at the lowest measurement frequency of 2340 MHz (= 9 mm). This setting promotes independent multipath fading at the grid points. $Rx_1$ remains fixed and is attached outside to the flat phantom. As $Tx_1$, an in-body insulated dipole is used that resonates at 2.457 GHz and is detailed in [2]. The dipole is polarized along the X-axis in Fig. 1. $Rx_1$ is a textile patch antenna with boresight along the Y-axis and pointing towards the phantom. $Rx_1$ is circularly polarized in the XZ-plane. The substrate of $Rx_1$ is a very flexible closed-cell expanded rubber protective foam. Ground plane and patch are fabricated using the 80-$\mu$m-thick conductive e-textile Flectron. A spacer made of foam is used to physically separate the conductive parts of $Rx_1$ from the phantom. Fig. 2 presents the $Rx_1$ antenna topology. Further technical specifications of $Rx_1$ can be found in [3].

The link between the on-body antenna $Tx_2$ (same location as $Rx_1$) and the antenna $Rx_2$ on an external terminal device at 2 m distance from the body is called 'hop 2'. The position of $Tx_2$ remains fixed while $Rx_2$ is moved along a 7 by 7 square grid with 7.5 cm spacing between the grid points. Again, this spacing is larger than half a wavelength at the lowest measurement frequency, this time in free space (= 6.4 cm). As $Tx_2$, a dipole antenna (2.450 GHz, polarization along the X-axis) is used. Furthermore, $Rx_2$ is a commercially available broadband discone antenna of type Electro-Metrics EM-6116 (2 to 10 GHz, polarization along the X-axis) [4].

Finally, the $S_{21}$ parameter is also measured for

---

*Department of Information Technology, Ghent University - iMinds, Gaston Crommenlaan 8 box 201, 9050 Ghent, Belgium, email: `wout.joseph@intec.ugent.be`.

†Department of Information Technology, Ghent University, Sint-Pietersnieuwstraat 41, 9000 Ghent, Belgium, email: `patrick.vantorre@ugent.be`.
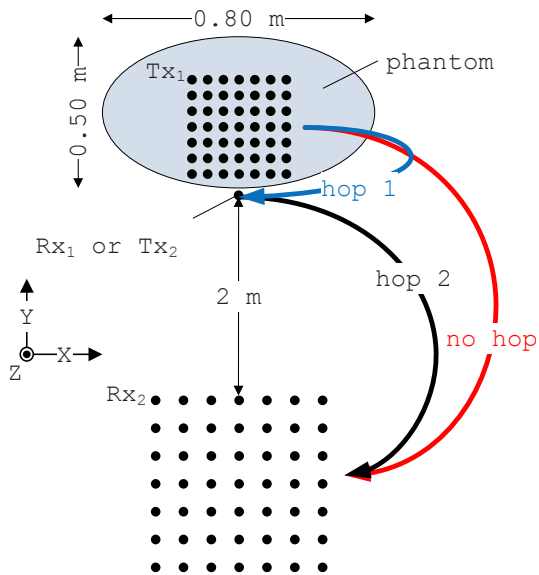
Figure 1: Measurement setup

the direct link between each of the 49 Tx$_1$ and each of the 49 Rx$_2$ positions, called 'no hop' in Fig. 1. Additionally, Fig. 3(a) shows a photograph of the measurement setup with indications of the equipment and the three different links under investigation. Fig. 3(b) shows a close-up of the phantom together with the transmitting and receiving antennas used for the 'hop 1' link.

The frequency range (2340 to 2620 MHz) was chosen because $|S_{11}|$ at the connectors of all the measurement antennas is less than -10 dB in this band, as shown in Fig. 4. The $S_{11}$ parameters in Fig. 4 were measured in correct conditions for the hospital scenario: Tx$_1$ was inside the tissue simu-
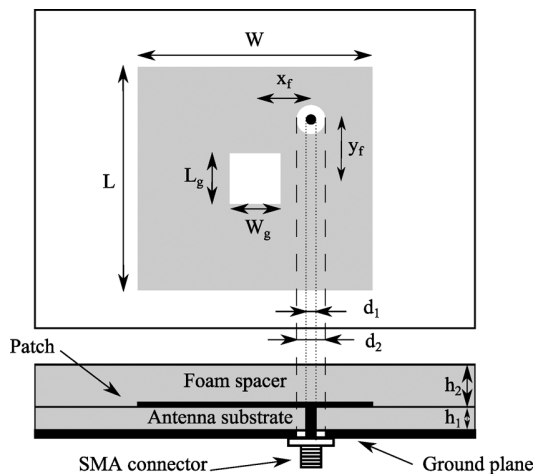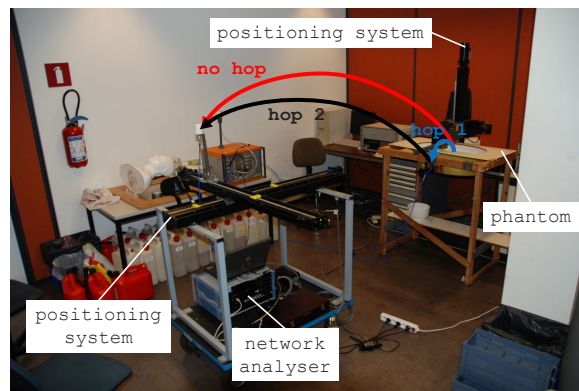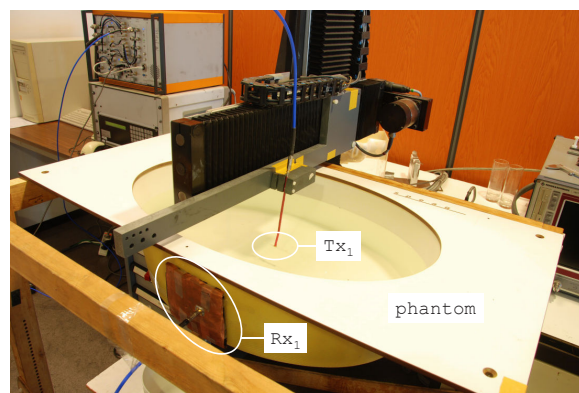


Figure 2: Topology of textile patch antenna Rx$_1$ (taken from [3])



(a) Entire setup



(b) Close-up of phantom

Figure 3: Photos of measurement setup

lating liquid, Rx$_1$ and Tx$_2$ were close to the liquid, and Rx$_2$ was located in free space.

Following measurements, the $S_{21}$ traces as function of frequency $f$ are converted to the delay domain by applying an Inverse Discrete Fourier Transform (IDFT) algorithm. Prior to the IDFT, $S_{21}(f)$ is multiplied by a Hann windowing function hann$(f)$ to suppress aliasing in the delay domain. A Hann window is considered to be a good trade-off between main-lobe width and side-lobe suppression. For each of the three communication links separately, the magnitude squared of the resulting channel impulse responses are spatially averaged over all Tx$_1$ and/or Rx$_2$ positions to form an APDP:

$$P(\tau) = 10 \log \left[ \text{avg} \left( \frac{|\text{IDFT}\left[\text{hann}(f) S_{21}(f)\right]|^2}{G^2} \right) \right] \tag{1}$$

In (1), $P(\tau)$ is an APDP in dB as function of delay $\tau$. The avg$(\cdot)$ operator represents the spatial averaging operation and $G$ is the coherent gain of the windowing function ($G = 0.5$ for the Hann window). For the three links, the spatial averaging in
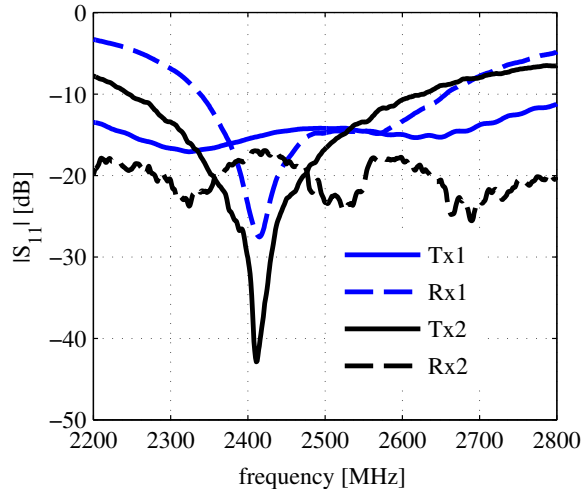
Figure 4: $|S_{11}|$ versus frequency of the measurement antennas



Figure 5: Averaged power delay profiles for the 'hop 1', 'hop 2', and 'no hop' links

(1) is done over at least 49 grid points. This is in agreement with [5], where 36 to 50 samples are suggested for an accurate estimation of the average.

## 3    Results

Fig. 5 shows the APDPs for the 'hop 1', 'hop 2', and 'no hop' links (delay resolution 3.57 ns, maximum delay 1   s). The 'hop 1' link is characterized by a steep descent of received power with delay, indicating a dominant Line-of-Sight (LoS) component. This is explained by the highly lossy (conductive) nature of the tissue simulating liquid prohibiting significant multipath propagation inside the phantom.

In Fig. 5, the power decay rate is similar for the 'hop 2' and 'no hop' links. The 'no hop' APDP is approximately a constant power shift down from the 'hop 2' APDP. It could therefore be concluded that the power reverberation for the 'hop 2' and 'no hop' links originates from the same propagation phenomena, namely reflections off the lab environment. This is further evidenced by the dirac-like 'hop 1' APDP: this link has a strong non-fading character that lacks significant multipath. The delay dispersion of 'hop 1' can therefore be neglected with respect to 'hop 2' and 'hop 1' is modeled well as a constant power attenuation.

The APDPs $P(\tau)$ are fitted to a linear decay of logarithmic power with delay (green lines in Fig. 5):

$$P(\tau) = a_0 + a_1 \cdot \tau \qquad (2)$$

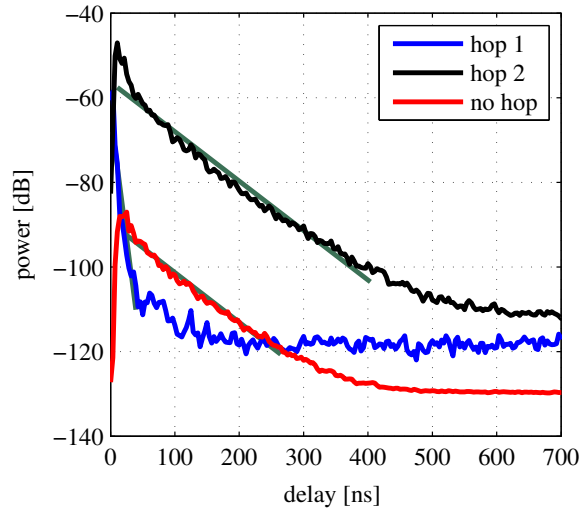The regression line (2) is fitted in the delay interval between the delay corresponding to the peak power (direct path) and the delay where the power drops below the measurement noise floor plus a noise margin of 10 dB. The measurement noise floor is determined at large delays where no multipath energy is present. The least-squares estimates of the regression parameters $a_0$ and $a_1$ are listed in Table 1. The path loss of the LoS component $-a_0$ amounts to 90 dB for the 'no hop' link. Despite the short distance between $Tx_1$ and $Rx_2$, the LoS path loss is relatively high and may even be too high to allow for reliable (low error rate) communication with realistic transceivers.

| link | $a_0$ [dB] | $a_1$ [dB/ns] |
|------|-----------|---------------|
| hop 1 | -63.90 | -1.18 |
| hop 2 | -56.30 | -0.12 |
| no hop | -89.60 | -0.12 |
| hop 1 * hop 2 | -112.21 | -0.13 |

Table 1: Regression parameters for 'hop 1', 'hop 2', 'no hop', and 'hop 1 * hop 2' links

Because the direct 'no hop' link might not be realistically feasible, we additionally investigated the scenario in which the data transmitted from $Tx_1$ to $Rx_1$ in 'hop 1' is relayed to $Rx_2$ through the 'hop 2' link. The relay channel between $Tx_1$ and $Rx_2$ is called 'hop 1 * hop 2' and its complex channel gain is calculated as $S_{21,\text{hop 1 * hop 2}}(f) = S_{21,\text{hop 1}}(f) S_{21,\text{hop 2}}(f)$. The APDPs of the 'no hop' and 'hop 1 * hop 2' links are compared in Fig. 6. Table 1 additionally lists the estimated linear regression parameters for the 'hop 1 * hop 2' link.

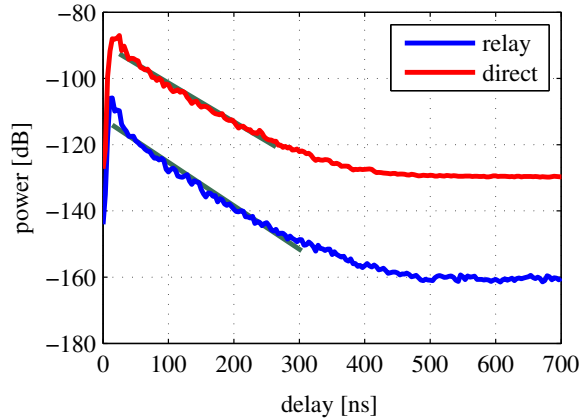The APDP for the 'hop 1 * hop 2' link is an al-

Figure 6: Averaged power delay profiles for the 'hop 1 * hop 2' and 'no hop' links

most constant 23 dB lower than for the 'no hop' link. Worse path loss performance for the relay link is expected as only propagation paths that arrive at/start from the on-body hub contribute to the received power at $Rx_2$, where this limitation does not exist for the direct 'no hop' link. However, the relay link offers options to improve the link budget. Packets arriving at the on-body hub through 'hop 1' can be amplified or retransmitted before being sent through 'hop 2'. Retransmission in particular would negate the highly lossy 'hop 1' link.

## 4   Conclusions and outlook

Power delay profiles for a wireless in-to-out-body endoscopy link have been investigated. Path loss for the direct link was found to be high to assure reliable communication. The dual-hop relay link suffered from even worse path loss, however this link type does offer additional options to alleviate the path loss issue through amplification or retransmission.

Furthermore, we considered a fixed location of the on-body antenna. In practice however, numerous locations can be chosen for the on-body antenna. Future research aims to also include the position of the on-body antenna on the circumference of the phantom as a parameter in the analysis.

## References

[1] CENELEC, "EN50383: basic standard for the calculation and measurement of electromagnetic field strength and SAR related to human exposure from radio base stations and fixed terminal stations for wireless telecommunication systems (110 MHz - 40 GHz)," September 2002.

[2] D. Kurup, W. Joseph, G. Vermeeren, and L. Martens, "Path loss model for in-body communication in homogeneous human muscle tissue," *IET Electronics Letters*, vol. 45, no. 9, pp. 453–454, April 2009.

[3] S. Agneessens, P. Van Torre, E. Tanghe, G. Vermeeren, W. Joseph, and H. Rogier, "On-body wearable repeater as a data link relay for in-body wireless implants," *IEEE Antennas and Wireless Propagation Letters*, vol. 11, pp. 1714–1717, 2013.

[4] http://www.electro-metrics.com/product/em-6116/105/.

[5] W. C. Y. Lee, *Mobile Communications Design Fundamentals*, 2nd ed. Wiley, 1993.